

First applications of Fayans functional to deformed nuclei

S V Tolokonnikov¹, I N Borzov², M Kortelainen^{3,4}, Yu S Lutostansky⁵, and E E Saperstein⁵

¹ Moscow Institute of Physics and Technology, Dolgoprudny and Kurchatov Institute, 123182 Moscow, Russia

E-mail: tolkn@mail.ru

² Joint Institute for Nuclear Research, 141980 Dubna, Russia

E-mail: ibor48@mail.ru

³ Department of Physics, P.O. Box 35 (YFL), University of Jyväskylä, FI-40014 Jyväskylä, Finland

⁴ Helsinki Institute of Physics, P.O. Box 64, FI-00014 University of Helsinki, Finland

E-mail: markus.kortelinen@jyu.fi

⁵Kurchatov Institute, 123182 Moscow, Russia

E-mail: lutostansky@yandex.ru

E-mail: saper43_7@mail.ru

PACS numbers: 21.60.Jz, 21.10.Ky, 21.10.Ft, 21.10.Re

Abstract. First calculations for deformed nuclei with the Fayans functional are carried out for the uranium and lead isotopic chains. The ground state deformations and deformation energies are compared to Skyrme-Hartree-Fock-Bogolyubov results of HFB-17 and HFB-27 functionals. For the uranium isotopic chain, the Fayans functional predictions are rather similar properties compared to HFB-17 and HFB-27. However, there is a disagreement for the lead isotopic chain. Both of the Skyrme HFB functionals predict rather strong deformations for the light Pb isotopes which does not agree with the experimental data on charge radii and magnetic moments of the odd Pb isotopes. On the other hand, the Fayans functional predicts a spherical ground state for all of the lead isotopes, in accordance with the data and the known in literature results obtained with the Gogny D1S force and SLy6 functional as well. The deformation energy curves are calculated and compared to four Skyrme functionals, SLy4, Sly6, SkM* and UNEDF1, for ²³⁸U nucleus and several lead deficient Pb isotopes. In the first case, the Fayans functional result is rather close to SkM* and UNEDF1 which, in particularly the latter one, describe the first and second barriers in ²³⁸U rather well. For the light lead isotopes, the Fayans deformation energy curves are qualitatively close to those of the SLy6 functional.

1. Introduction

A long-standing goal of the low-energy nuclear theory community is to have a unified theoretical framework, applicable to nuclear structure and reactions. Presently, due to computational limitations, *ab initio* approaches are applicable to light or medium mass closed-shell nuclei only. Therefore, microscopical theories which use effective forces with phenomenological parameters are usually applied to describe the entire nuclear chart. The nuclear density functional theory (DFT) being the most popular of such kind of models. In the framework of nuclear DFT, complex many-body correlations are encoded into the energy density functional (EDF), constructed from the nuclear densities and currents. Historically, since the work by Vautherin and Brink [1], the Hartree-Fock (HF) method with the effective Skyrme forces has become very popular in the nuclear physics. From the very beginning, the Skyrme HF method was aimed at calculating global properties of nuclei, such as the binding energy and neutron and proton density distributions. A little later the HF method with the effective Gogny force was suggested [2] and successfully applied to the same objects as the Skyrme HF method. In addition to these, relativistic mean-field (RMF) models have been also employed in the nuclear physics, see Ref. [3] and references therein. In fact, it was quite soon realized that these methods had a rather strong correspondence to DFT methods employed e.g. in atomic physics. Indeed, during the last few decades, mean-field methods in the framework of HF and Hartree-Fock-Bogolyubov (HFB) theory, have been widely used in the nuclear physics [4, 5]. The HFB, a method suitable for superfluid nuclei with pairing correlations, is a generalization of the HF, which allows particles and holes to be treated on the equal footing.

The use of density-dependent effective interactions is a common feature of these mean-field approaches. When Skyrme and Gogny effective forces are written as a form of the EDF, a rather simple ansatz for density dependence is assumed. Schematically it reads

$$E_0^{\text{int}}[\rho] = \int \mathcal{E}(\rho(\mathbf{r})) d^3r = \int \frac{a\rho^2}{2} (1 + \alpha\rho^\sigma) d^3r, \quad (1)$$

where $\rho(\mathbf{r})$ is the matter density and a , b , and $\sigma \leq 1$ are parameters. For brevity, we omit for a time the isotopic indices and do not discuss the spin-orbit and other “small” terms of the effective force. As will be later discussed, Fayans functional has more sophisticated density dependence [6, 7, 8, 9, 10]. Recently, density dependence of Skyrme-like EDFs has been enriched by utilizing density matrix expansion techniques [11, 12, 13, 14, 15, 16].

The parameters of Skyrme forces, as well as Gogny and RMF models, have been typically adjusted to the experimental data on nuclear binding energies and charge radii. Many optimization schemes also use data on single-particle levels, fission properties, together with other observables and pseudo-observables. Because data on very neutron rich nuclei are scarce, especially at the time when some of the older Skyrme parameterizations were adjusted, some of the isovector parameters may have larger

uncertainties. The best description of nuclear masses (the root-mean-square deviation from the respective experimental values being smaller than 600 keV) was attained with the HFB-17 EDF by the Brussels-Montreal Collaboration [17, 18]. This result was achieved, however, by including some phenomenological corrections atop of the mean field.

The Fayans functional [6, 7, 8, 9, 10] used in this work assumes a rather sophisticated density dependence which can be schematically written as

$$\mathcal{E}(\rho) = \frac{a\rho^2}{2} \frac{1 + \alpha\rho^\sigma}{1 + \gamma\rho}. \quad (2)$$

The use of the bare mass, i.e. $m^* = m$, is another peculiarity of the Fayans functional. Both of these features of the Fayans approach are connected to the self-consistent theory of finite Fermi systems (TFFS) [19].

Up to now, all applications of the Fayans functional were limited to spherical nuclei. In addition to the above mentioned, they included the analysis of charge radii [20], of the magnetic [21, 22] and quadrupole [23, 24] moments in odd nuclei, of characteristics of the first 2^+ excitations in even semi-magic nuclei [25, 26] and of beta-decay [27] as well. Recently, single-particle spectra of magic nuclei were analyzed [28]. In all aforementioned cases, a reasonable description of the data was achieved, better as a rule than in analogous Skyrme HFB calculations.

The aim of this work is to apply for the first time the Fayans functional to deformed nuclei. The principle goal is to study deformation properties of Fayans functional in selected set of isotopic chains. This paves a way for more comprehensive studies with the Fayans functional across the nuclear chart. This article is organized as follows: In Section II, the path from the self-consistent TFFS to the Fayans functional is outlined. In Section III, the version FaNDF⁰ [9] of the Fayans functional is briefly described. Section IV deals with empirical arguments against stable deformations in the ground states of the light lead isotopes. Calculated results for U and Pb isotopes are presented in Section V, and in Section VI we draw our conclusions.

2. Self-consistent TFFS and the Fayans functional

The self-consistent TFFS [19] is based on the general principles of TFFS [29] supplemented with the condition of the self-consistency in the TFFS between the energy-dependent mass operator $\Sigma(\mathbf{r}_1, \mathbf{r}_2; \varepsilon)$, the single-particle Green's function $G(\mathbf{r}_1, \mathbf{r}_2; \varepsilon)$, and the effective NN interaction $\mathcal{U}(\mathbf{r}_1, \mathbf{r}_2, \mathbf{r}_3, \mathbf{r}_4; \varepsilon, \varepsilon')$ [30].

This approach starts from the quasiparticle mass operator $\Sigma_q(\mathbf{r}_1, \mathbf{r}_2; \varepsilon)$ which, by definition [29], coincides with the exact mass operator Σ at the Fermi surface. In the mixed coordinate-momentum representation the operator $\Sigma_q(\mathbf{r}, k^2; \varepsilon)$ depends linearly on the momentum square k^2 and the energy ε [29, 19],

$$\Sigma_q(\mathbf{r}, k^2; \varepsilon) = \Sigma_0(\mathbf{r}) + \frac{1}{2m\varepsilon_F^0} \mathbf{k} \Sigma_1(\mathbf{r}) \mathbf{k} + \Sigma_2(\mathbf{r}) \frac{\varepsilon}{\varepsilon_F^0}, \quad (3)$$

where $\varepsilon_F^0 = (k_F^0)^2/2m$ is the Fermi energy of nuclear matter, k_F^0 being the corresponding Fermi momentum. By definition, we have

$$\Sigma_1(\mathbf{r}) = \varepsilon_F^0 \left. \frac{\partial \Sigma(\mathbf{r}, k^2; \varepsilon)}{\partial \varepsilon_k} \right|_0, \quad (4)$$

$$\Sigma_2(\mathbf{r}) = \varepsilon_F^0 \left. \frac{\partial \Sigma(\mathbf{r}, k^2; \varepsilon)}{\partial \varepsilon} \right|_0, \quad (5)$$

where $\varepsilon_k = k^2/2m$ and the subscribe “0” means that the energy and momentum variables are taken at the Fermi surface. Thus, the component Σ_2 determines the Z -factor:

$$Z(\mathbf{r}) = (1 - \Sigma_2(\mathbf{r})/\varepsilon_F^0)^{-1}, \quad (6)$$

whereas the inverse effective mass is

$$\frac{m}{m^*(\mathbf{r})} = \frac{(1 + \Sigma_1(\mathbf{r})/\varepsilon_F^0)}{(1 - \Sigma_2(\mathbf{r})/\varepsilon_F^0)}. \quad (7)$$

Usually, the quantity inverse to the numerator is called the “ k -mass”, and the denominator, the “ E -mass”.

The wave functions $\psi_\lambda(\mathbf{r})$ which diagonalize the quasiparticle Green function $G_q = (\varepsilon - \varepsilon_k - \Sigma_q)^{-1}$ obey the following equation

$$\left(\Sigma_0(\mathbf{r}) - \frac{1}{2m\varepsilon_F^0} \nabla \Sigma_1(\mathbf{r}) \nabla + \Sigma_2(\mathbf{r}) \frac{\varepsilon_\lambda}{\varepsilon_F^0} \right) \psi_\lambda = \varepsilon_\lambda \psi_\lambda. \quad (8)$$

They are orthonormalized with the weight,

$$\int d\mathbf{r} \psi_\lambda^*(\mathbf{r}) \psi_{\lambda'}(\mathbf{r}) (1 - \Sigma_2(\mathbf{r})) = \delta_{\lambda\lambda'}. \quad (9)$$

The Lagrange formalism was used in Ref. [19], with the quasiparticle Lagrangian L_q being constructed in such a way that the corresponding Lagrange equations coincide with Eq. (8).

In the double-magic nuclei, which are non-superfluid, the Lagrangian density \mathcal{L}_q , $L_q = \int d\mathbf{r} \mathcal{L}_q(\mathbf{r})$, depends on three sorts of densities $\nu_i(\mathbf{r})$, $i = 0, 1, 2$:

$$\nu_0(\mathbf{r}) = \sum n_\lambda \psi_\lambda^*(\mathbf{r}) \psi_\lambda(\mathbf{r}), \quad (10)$$

$$\nu_1(\mathbf{r}) = -\frac{1}{2m\varepsilon_F^0} \sum n_\lambda \nabla \psi_\lambda^*(\mathbf{r}) \nabla \psi_\lambda(\mathbf{r}), \quad (11)$$

$$\nu_2(\mathbf{r}) = \frac{1}{\varepsilon_F^0} \sum n_\lambda \varepsilon_\lambda \psi_\lambda^*(\mathbf{r}) \psi_\lambda(\mathbf{r}), \quad (12)$$

where ε_λ and n_λ are the quasiparticle energies and occupation numbers, $n_\lambda = (0, 1)$. Evidently, one gets

$$\nu_0(\mathbf{r}) = Z(\mathbf{r})\rho(\mathbf{r}), \quad (13)$$

where the density $\rho(\mathbf{r})$ is normalized to the total particle number. The relation between $\nu_1(\mathbf{r})$ and the Skyrme density $\tau(\mathbf{r})$ is more complicated [19]. The density $\nu_2(\mathbf{r})$ has no analogue in the Skyrme HF theory.

The components Σ_i of the mass operator (3) can be found from the interaction Lagrangian $L'_q[\nu_i]$ as follows:

$$\Sigma_i = \frac{\delta L'_q}{\delta \nu_i}. \quad (14)$$

The simplest ansatz for the quasiparticle Lagrangian which involves the momentum and energy dependence effects on equal footing was suggested in [19]:

$$\mathcal{L}'_q = -C_0 \left(\frac{1}{2} \nu_0 \hat{\lambda}_{00} \nu_0 + \frac{\gamma}{6\rho_0} \nu_0^3 + \hat{\lambda}_{01} \nu_0 \nu_1 + \hat{\lambda}_{02} \nu_0 \nu_2 \right), \quad (15)$$

where $C_0 = (dn/d\varepsilon_F)^{-1} = \pi^2/(p_F m)$ is the usual TFFS normalization factor, inverse density of states at the Fermi surface, and $\rho_0 = (k_F^0)^3/3\pi^2$ is the density of one kind of nucleons in equilibrium symmetric nuclear matter. The amplitudes

$$\hat{\lambda}_{ik} = \lambda_{ik} + \lambda'_{ik} \tau_1 \tau_2 \quad (16)$$

are the isotopic matrices and only one of them,

$$\hat{\lambda}_{00}(\mathbf{r}_1, \mathbf{r}_2) = \hat{\lambda}_{00}(1 + r_0^2 \Delta_1) \delta(\mathbf{r}_1, \mathbf{r}_2), \quad (17)$$

is the finite range operator. The term proportional to γ , in Eq. (15), results in the density dependence of the main, scalar and isoscalar, Landau–Migdal interaction amplitudes [29].

To minimize the number of new parameters, the ansatz $\lambda'_{01} = \lambda'_{02} = 0$ was used in [19]. In this case, the components Σ_1^τ and Σ_2^τ of the mass operator do not depend on τ , being the function of the total density $\nu_0^+ = \nu_0^n + \nu_0^p$:

$$\Sigma_1^\tau(\mathbf{r}) = \frac{\delta L_q}{\delta \nu_2^\tau(\mathbf{r})} = C_0 \lambda_{01} \nu_0^+(\mathbf{r}), \quad (18)$$

$$\Sigma_2^\tau(\mathbf{r}) = \frac{\delta L_q}{\delta \nu_2^\tau(\mathbf{r})} = C_0 \lambda_{02} \nu_0^+(\mathbf{r}). \quad (19)$$

With the use of (13) and (19), one can obtain the explicit dependence of the Z -factor on the density with the usual normalization:

$$Z_\tau(\mathbf{r}) = \frac{2}{1 + \sqrt{1 - 4C_0 \lambda_{02} \rho^+(\mathbf{r})/\varepsilon_F^0}}. \quad (20)$$

The total interaction energy can be found for the Lagrangian (15) according the canonical rules. It corresponds to the following EDF:

$$\mathcal{E}_{\text{int}} = C_0 \left[\frac{1}{2} \hat{\lambda}_{00} (\nu_0^2 - r_p^2 (\nabla \nu_0)^2) + \hat{\lambda}_{01} \nu_0 \nu_1 + \frac{\gamma}{6\rho_0} \nu_0^3 \right]. \quad (21)$$

It does not contain the “new” density ν_2 and converts to the Skyrme EDF at limit $\nu_0 \rightarrow \rho$ and $\nu_1 \rightarrow \tau$. However, the substitution of Eq. (13) with the Z -factor (20) results in rather sophisticated EDF in the self-consistent TFFS, which hardly can be introduced *ad hoc*.

The parameters of the Lagrangian (15) were found in [19] by fitting binding energies, charge radii and single-particle spectra of double-magic nuclei from ^{40}Ca to ^{208}Pb . The

found values $\lambda_{01} = 0.31$ and $\lambda_{02} = -0.25$ correspond to the following characteristics of nuclear matter: $m_0^* = 0.95m$ and $Z_0 = 0.8$. The latter agrees with the value found in [31] on the base of the dispersion relation for the quantity $\partial\Sigma/\partial\varepsilon$ [29] in nuclear matter.

In Ref. [6] the so-called Generalized EDF method was formulated as a generalization of the Kohn–Sham (KS) method [32] for superfluid nuclei. In this case, the EDF depends not only on the normal densities $\rho_{n,p}(\mathbf{r})$, but on their anomalous counterparts $\nu_{n,p}(\mathbf{r})$ as well. Independently, similar development of the KS method was suggested in condensed matter physics [33]. The pairing problem was considered in [6] with an elegant method of direct solving Gor’kov equations for spherical systems in the coordinate representation [34]. In practice, this method is close to solving HFB equations which was made firstly in [2] for the Gogny EDF and in [35] for the Skyrme EDF.

The KS method is based on the Hohenberg–Kohn theorem [36] stating that the ground state energy of a Fermi system is a functional of its density. Unfortunately, this theorem does not give any recipe to construct the EDF. Fayans *et al.* [6] found that the EDF (21) can be rather accurately approximated with a rational ρ -dependence of Eq. (2) type. In addition, they used the ansatz $m^* = m$ typical for the KS method. This also agrees well with the above estimation. Thus, the Fayans functional can be interpreted as a simplified version of the self-consistent TFFS [19] and the “denominator” in the EDF (2) appears due to the energy dependence effects taken into account in the TFFS.

It is worth to mention that the use of any EDF with density dependence leads to serious problems if one tries to go beyond mean-field multi-reference calculations, such as particle number projection or angular momentum projection [37, 38, 39, 40]. Therefore, in this work, we use Fayans functional for single-reference calculations only.

Three sets of the EDF parameters, DF1–DF3, were suggested in Ref. [8], but the most part of calculations with Fayans EDF were carried out with the set DF3 [10] or its version DF3a for transuranium region [41]. Although up to now there are no systematic calculations of nuclear binding energies across the whole nuclear chart within this method, isotopic chains of spherical nuclei were examined in [10, 41, 20]. It was found that the accuracy is only a little worse than that of the best Skyrme HFB calculations. As for the accuracy of reproducing the charge radii [20] of spherical nuclei, typical deviation is of the order of 0.01–0.02 fm, i.e. the agreement is on the par or higher compared to Skyrme EDF models. This may be linked to more adequate density dependence of the Fayans EDF compared to the Skyrme one. Indeed, if we denote the average error in describing the binding energies as $\overline{\delta E}$ and that for the charge radii as $\overline{\delta R_{\text{ch}}}$, these quantities should be, due to the Hohenberg–Kohn theorem [36], proportional to each other,

$$\overline{\delta R_{\text{ch}}} = \alpha \overline{\delta E}, \quad (22)$$

where the coefficient α depends on the functional we use. As the analysis of [20] showed, for the Fayans EDF this coefficient is less than those of the HFB-17 and SLy4 functionals. Again, this observation may be linked to more enriched density dependence of Fayans functional, which allows to incorporate complex many-body correlations more

efficiently. Fayans EDF provides also a high quality description of magnetic [21, 22] and quadrupole [23, 24] moments of odd spherical nuclei, energies and $B(E2)$ values in even semi-magic nuclei [25, 26]. Recent analysis [28] of the single-particle energies of double-magic nuclei with the Fayans functional *vs* the HFB-17 one also evidences in favor of the first one.

Up to now, all self-consistent calculations with Fayans functionals were carried out for spherical nuclei only. In Ref. [41] deformations for the transuranium nuclei were taken into account approximately. This work presents the first application of Fayans functional to axially deformed nuclei.

3. FaNDF⁰ functional

For completeness, we write down explicitly main ingredients of the Fayans EDF method. In this method, the ground state energy of a nucleus is considered as a functional of normal and anomalous densities,

$$E_0 = \int \mathcal{E}[\rho(\mathbf{r}), \nu(\mathbf{r})] d^3r, \quad (23)$$

where the isotopic indices and the spin-orbit densities are for brevity omitted.

Main distinctions between this method and the Skyrme EDF approach are located in the normal part of the EDF $\mathcal{E}_{\text{norm}}$, containing the central and spin-orbit terms, and Coulomb interaction term for protons. In the major part of applications of this method [7, 8, 10], the DF3 functional was used with the finite range Yukawa-type central force. In this work we use the EDF FaNDF⁰ from [9] with a localized form of the Yukawa function, $\text{Yu}(r) \rightarrow 1 - r_c^2 \nabla^2$, which makes the structure of the surface part of the EDF closer to that of the Skyrme functionals. This form allows us to use a modified version of computer code HFBTHO [42], originally constructed for Skyrme-like EDFs. The parameters of FaNDF⁰ were fitted to the equation of state of nuclear and neutron matter by Friedman and Pandharipande [43] and masses of lead and tin isotopes.

The volume part of the EDF, $\mathcal{E}^v(\rho)$, is taken as a fractional function of densities $\rho_+ = \rho_n + \rho_p$ and $\rho_- = \rho_n - \rho_p$:

$$\mathcal{E}^v(\rho) = C_0 \left[a_+^v \frac{\rho_+^2}{2} f_+^v(x) + a_-^v \frac{\rho_-^2}{2} f_-^v(x) \right], \quad (24)$$

where

$$f_+^v(x) = \frac{1 - h_{1+}^v x^\sigma}{1 + h_{2+}^v x^\sigma} \quad (25)$$

and

$$f_-^v(x) = \frac{1 - h_{1-}^v x}{1 + h_{2-}^v x}. \quad (26)$$

Here, $x = \rho_+/(2\rho_0)$ is the dimensionless nuclear density. The power parameter $\sigma = 1/3$ is chosen in the FaNDF⁰ functional, in contrast to DF3 where $\sigma = 1$ is used. The structure of other terms in the volume parts of these two functionals is kept the same. However,

the above mentioned difference leads to significantly different values of the dimensionless parameters in Eqs. (24) – (26) although they still correspond to the same characteristics of nuclear matter, the incompressibility $K_0 = 220$ MeV, equilibrium density $2\rho_0 = 0.16$ fm $^{-3}$ ($r_0 = 1.143$ fm), and energy per particle $\mu = -16.0$ MeV. Parameters denoted by “+” are $a_+^v = -9.559$, $h_{1+}^v = 0.633$, $h_{2+}^v = 1.300$, and parameters denoted by “-” are $a_-^v = 4.428$, $h_{1-}^v = 0.25$, $h_{2-}^v = 1.300$, which all are dimensionless quantities. This parameter set corresponds to the asymmetry energy coefficient of $a_{\text{sym}} = 30.0$ MeV.

The main difference between FaNDF 0 and DF3 functionals is in the structure of the surface term. Now it is as follows

$$\mathcal{E}^s(\rho) = C_0 \frac{1}{4} \frac{a_+^s r_0^2 (\nabla \rho_+)^2}{1 + h_+^s x^\sigma + h_{\nabla}^s r_0^2 (\nabla x_+)^2}, \quad (27)$$

with $h_+^s = h_{2+}^v$, $a_+^s = 0.600$, $h_{\nabla}^s = 0.440$.

The usual form for the direct Coulomb term of the EDF of Ref. [9] is employed, the folded charge density ρ_{ch} is found with taking into account the proton and neutron form factors. As to the exchange Coulomb term, it was taken as follows

$$-\frac{3}{4} \left(\frac{3}{\pi} \right)^{1/3} e^2 \rho_p^{4/3} (1 - h_{\text{Coul}} x_+^\sigma), \quad (28)$$

with $h_{\text{Coul}} = 0.941$. Such a strong suppression in comparison with the Slater approximation with $h_{\text{Coul}} = 0$ helps to solve the so-called Nollen–Shiffer anomaly [44]. It is worth to mention that similar suppression of the Coulomb exchange term was made in some Skyrme functionals [45].

The usual for the TFFS [29] structure of the spin-orbit term was used in FaNDF 0 with the same spin-orbit parameters as in the DF3 functional [10].

For completeness, we write down explicitly the anomalous term of the EDF [9],

$$\mathcal{E}_{\text{anom}} = C_0 \sum_{i=n,p} \nu_i^\dagger(\mathbf{r}) f^\xi(x_+(\mathbf{r})) \nu_i(\mathbf{r}), \quad (29)$$

where the density dependent dimensionless effective pairing force is

$$f^\xi(x_+) = f_{\text{ex}}^\xi + h^\xi x_+ + f_{\nabla}^\xi r_0^2 (\nabla x_+)^2, \quad (30)$$

with $f_{\text{ex}}^\xi = -2.8$, $h^\xi = 2.8$, $f_{\nabla}^\xi = 2.2$.

All above values of the parameters were found in Ref. [9] by fitting the masses and charge radii of approximately one hundred spherical nuclei from calcium isotopes to lead isotopes.

In our current implementation of the Fayans functional to the computer code HFBTHO, due to technical reasons, we made two small simplifications to the original FaNDF 0 EDF. Firstly, we used the approximation $\rho_{\text{ch}} = \rho_p$ for the direct Coulomb term. Secondly, we put $f_{\nabla}^\xi = 0$ in (30) making the anomalous EDF closer to that used in [10]. Therefore below we use the above parameters for the normal part of the EDF only. As to the anomalous EDF, the parameters will be found anew and will be given in the corresponding places. As far as we deal with the zero-range pairing force, the strength parameters depend on the cutoff energy E_{cut} in the pairing problem, being also

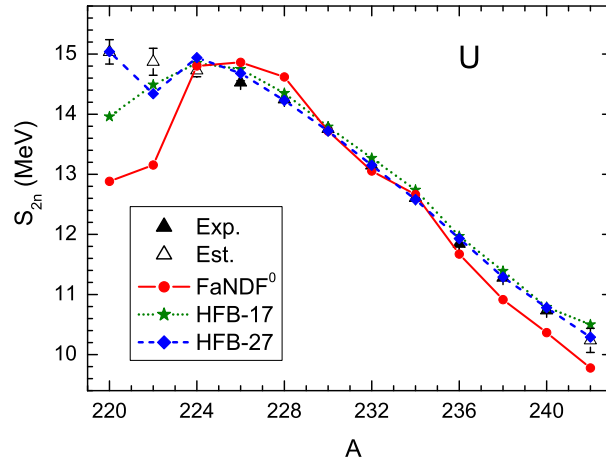


Figure 1. (Color online) Two-neutron separation energies S_{2n} for even U isotopes. Predictions of the FaNDF⁰ functional are compared to two Skyrme EDFs HFB-17 and HFB-27. Empty triangles show the estimated values [57].

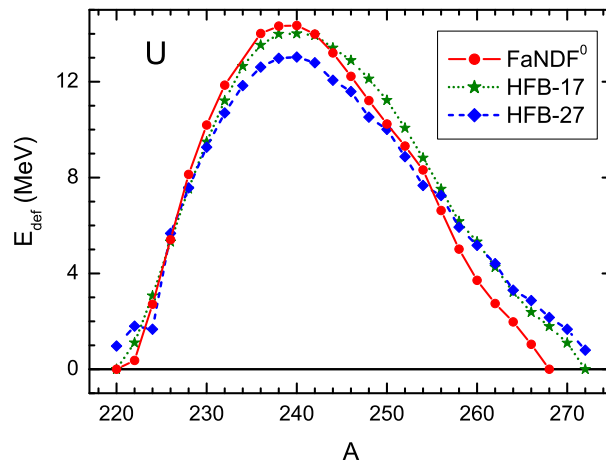


Figure 2. (Color online) Deformation energy E_{def} for even U isotopes. Predictions of the FaNDF⁰ functional are compared to two Skyrme EDFs HFB-17 and HFB-27.

smoothly A dependent [10]. In practice, this means that we take $f^\xi = -0.220$ for U and $f^\xi = -0.224$ for Pb isotopes.

4. Results

4.1. Uranium chain

We have chosen uranium isotopes for the first application of the FaNDF⁰ EDF to deformed nuclei, since most of them have a well established stable deformation. There has been numerous Skyrme EDF studies about the deformation landscape of actinide nuclei, see e.g. [46, 47, 48, 49] to list only a few of the recent ones.

In this work, due to employed axial computer code, we limit ourselves to the

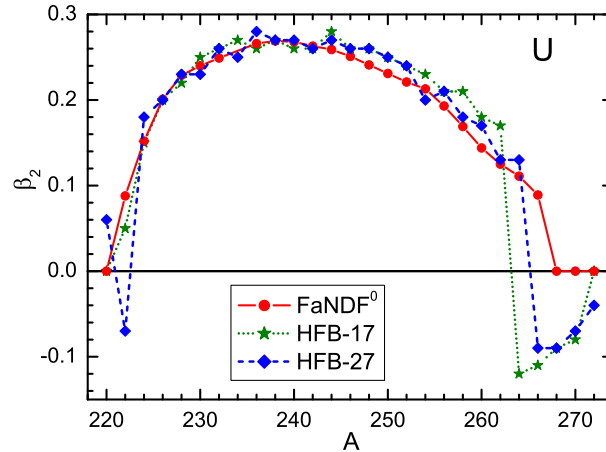


Figure 3. (Color online) Quadrupole deformation parameter for even U isotopes. Predictions of the FaNDF^0 functional are compared to two Skyrme EDFs HFB-17 and HFB-27.

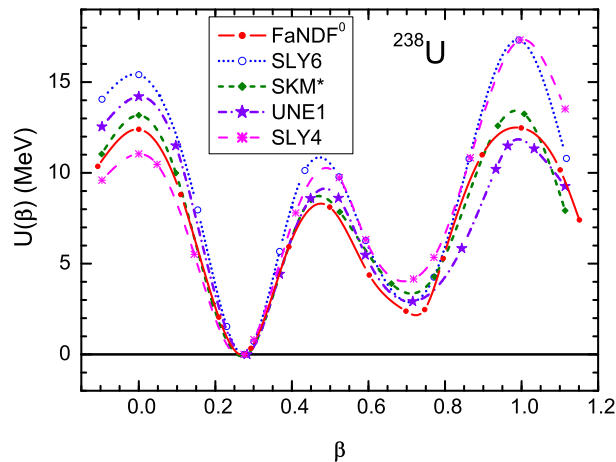


Figure 4. (Color online) The deformation energy curve for ^{238}U . Predictions of the FaNDF^0 functional are compared to four Skyrme EDFs. UNE1 label refers to the UNEDF1 EDF.

quadrupole deformation β_2 only, with reflection symmetry assumed. We have mainly focused on the ground state characteristics which are, unlike the fission barriers, within the reach of the current axial framework. Indeed, the ground states of U isotopes are expected to be axially deformed. Tri-axial deformation, which usually appears at the top of the fission barriers, is neglected in the present study. Also, the role of octupole degrees of freedom becomes important around the second fission barrier in the case of asymmetric fission. For the ground states of uranium isotopes we present a systematic comparison of our results to those of two versions of Skyrme HFB functionals, HFB-17 and HFB-27 [18].

For the uranium chain, we find our results converged when number of the oscillator shells is equal to $N_{\text{sh}} = 25$, i.e. the change of this number to $N_{\text{sh}} = 30$ does not

practically influences the results. As to the pairing force, the set of [9] with $f_{\text{ex}}^\xi = -h^\xi$ corresponds to the “surface” pairing with a strong attraction at the surface and very small value of f^ξ inside a nucleus. Such model of pairing is typical for all versions of the Fayans functional [10, 25]. Here we have found that the deformation energy for surface pairing is very close to that for the “volume” pairing model (corresponding to $h^\xi = 0$), provided the deformation parameter β_2 is less than $0.3 \div 0.5$. To stress the effect of the specific density dependence of the normal part of the Fayans EDF, we use as a rule the simplest one parameter volume pairing. The cutoff energy $E_{\text{cut}} = 60$ MeV is chosen, with corresponding value $f^\xi = -0.220$ fitted to double mass differences for the uranium isotopes.

In figure 1, two-neutron separation energies

$$S_{2n}(N, Z) = B(N, Z) - B(N - 2, Z), \quad (31)$$

are shown for uranium isotopes. Comparison is made with experimental data [57] and predictions of the HFB-17 and HFB-27 EDFs. Taking into account that the parameters of the FaNDF⁰ functional were fitted only for spherical nuclei not heavier than the lead, the description of S_{2n} values for uranium isotopes looks rather reasonable. In figures 2 and 3, a comparison is presented to the same Skyrme functionals for the deformation energy,

$$E_{\text{def}}(\beta_2) = B(\beta_2) - B(\beta_2 = 0), \quad (32)$$

and the deformation parameter itself. Unfortunately, both of these quantities have no direct experimental equivalent. We see that our calculations with the FaNDF⁰ functional reasonably agree with both the Skyrme EDF predictions.

To examine the applicability of the FaNDF⁰ functional for description of large deformations, we have calculated deformation energy curve for ²³⁸U nucleus up to the second fission barrier, shown in figure 4. For the comparison we also show the results obtained with SLy6 [50], SkM* [51], UNEDF1 [48], and SLy4 [50] Skyrme EDFs. All calculations were carried out within the same calculation scheme, i.e. with account for the quadrupole deformation only, without tri-axiality or octupole degrees of freedom. By neglecting these degrees of freedom, calculated inner fission barriers are typically raised by a few MeV and outer fission barriers, in asymmetric fission, substantially more, see e.g. [52]. Therefore, it is not meaningful to compare numerical values of the barriers in figure 4 with experimental values directly. However, it is worth to note that the FaNDF⁰ curve is rather close to SkM* and UNEDF1 ones which both, in particularly the UNEDF1, after inclusion of tri-axial and octupole degrees of freedom, describe uranium barriers reasonable well [48]. On the basis of the results obtained for the uranium isotopes, it seems reasonable to apply this functional for the analysis of the deformation characteristics of other isotopic chains.

4.2. Lead chain

Our interest to the lead chain is motivated with the observation that HFB-27 and other functionals of this family predict [18] rather strong deformations, $|\beta_2| \simeq 0.2 \div 0.3$, for

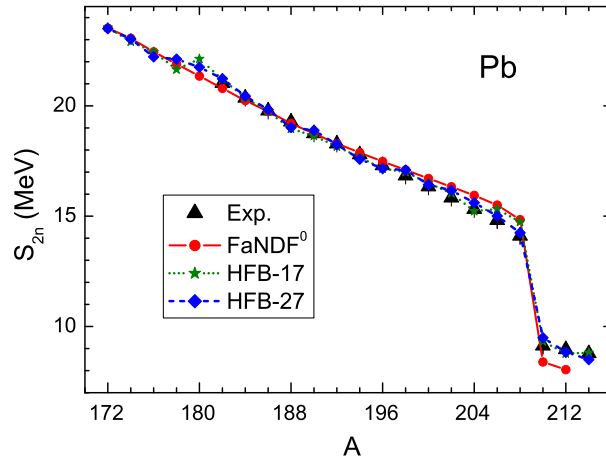


Figure 5. (Color online) Two-neutron separation energies S_{2n} for even Pb isotopes. Predictions of the FaNDF⁰ functional are compared to two Skyrme EDFs HFB-17 and HFB-27.

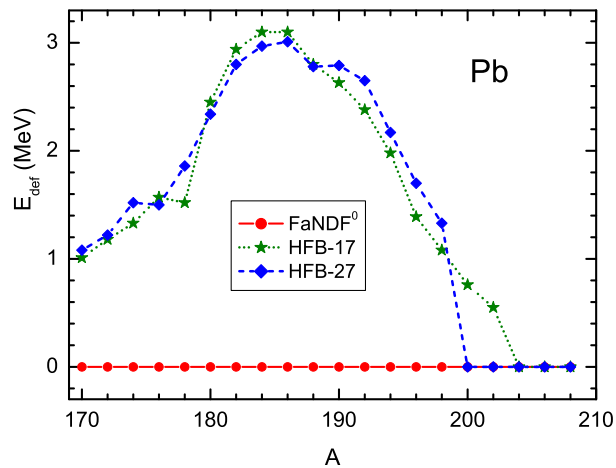


Figure 6. (Color online) Deformation energy E_{def} for even Pb isotopes. Predictions of the FaNDF⁰ functional are compared to two Skyrme EDFs HFB-17 and HFB-27.

light $^{180-192}\text{Pb}$ isotopes. Also, many other Skyrme EDFs seem to predict, at the mean-field level, the appearance of the deformation at the region of light Pb isotopes, see e.g. [53, 54] In our opinion, this does not correspond to the trend of the empirical data on charge radii [20] or magnetic moments [21, 22]. Indeed, charge radii produced by the HFB-27 EDF [18] describes the data for heavy Pb isotopes perfectly well but disagree significantly for those lighter than ^{192}Pb . Analysis of Ref. [55] within the Generator Coordinate Method with the use of the Gogny force D1S and of Ref. [56] with the SLy6 EDF confirmed the spherical form for these neutron deficient Pb isotopes. Although in both studies, the angular momentum projection technique was used, the simplest mean-field calculation also did not predict so large deformations as in [18]. Thus predictions of different Skyrme functionals for the light Pb isotopes are essentially different. Therefore it is of interest to look how the FaNDF⁰ functional behaves for these nuclei and compare

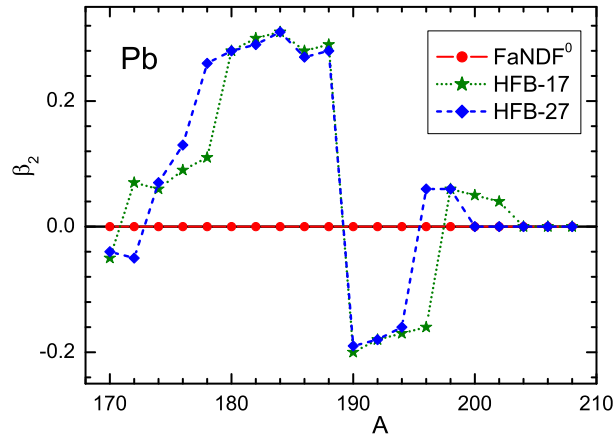


Figure 7. (Color online) Quadrupole deformation parameter for even Pb isotopes. Predictions of the FaNDF⁰ functional are compared to two Skyrme EDFs HFB-17 and HFB-27.

our predictions with those of various Skyrme EDFs.

In the analysis of the lead isotopes, we use the same calculation scheme as for the uranium chain, i.e. $N_{\text{sh}} = 25$ and $E_{\text{cut}} = 60$ MeV is chosen, and the corresponding value $f^\xi = -0.224$ being a bit different to describe better S_n and S_{2n} values. We again begin with the two-neutron separation energies S_{2n} , shown in figure 5. On average, agreement with the data with FaNDF⁰ is only a little worse compared to the HFB-17 and HFB-27 functionals.

As to the deformation characteristics, there is a notable difference between predictions of the Fayans FaNDF⁰ EDF and those of the two Skyrme functionals under consideration. Namely, calculations with the Fayans functional result to a spherical mean-field ground state for all of the lead isotopes. At the same time, both of HFB-17 and HFB-27 functionals predict a stable deformation in the ground states for many light Pb isotopes, as shown in figure 7. For the HFB-27 functional, deformation appears for isotopes with $A = 170 \div 198$, and for the HFB-17 functional, for all isotopes with $A < 204$. For both the functionals, the deformation changes sign from positive for ^{188}Pb to negative for ^{190}Pb , and the deformation is strong for isotopes with $A = 180 \div 192$, $\beta_2 \simeq 0.3$ for $A = 180 \div 188$ and $\beta_2 \simeq -0.2$ for $A = 190 \div 194$ in the case of HFB-27 functional and for $A = 190 \div 196$ in the case of HFB-17 one. Thus, the the value of the deformation parameter within this mass-region is approximately of the same order of magnitude as for the uranium isotopes. The deformation energy is less, $E_{\text{def}} \simeq 3$ MeV, also not negligible, as shown in figure 6. To summarize, the predictions of both these HFB functionals do not follow experimental data trend on charge radii and magnetic moments as it was discussed above. In addition, they disagrees with the predictions of Ref. [56] for the SLy6 EDF.

To investigate the problem in more detail, we have calculated the deformation energy curves $U(\beta)$ for several light Pb isotopes with the FaNDF⁰ functional and the same Skyrme EDFs, as for the case of ^{238}U . The results are shown in figure 8. We begin

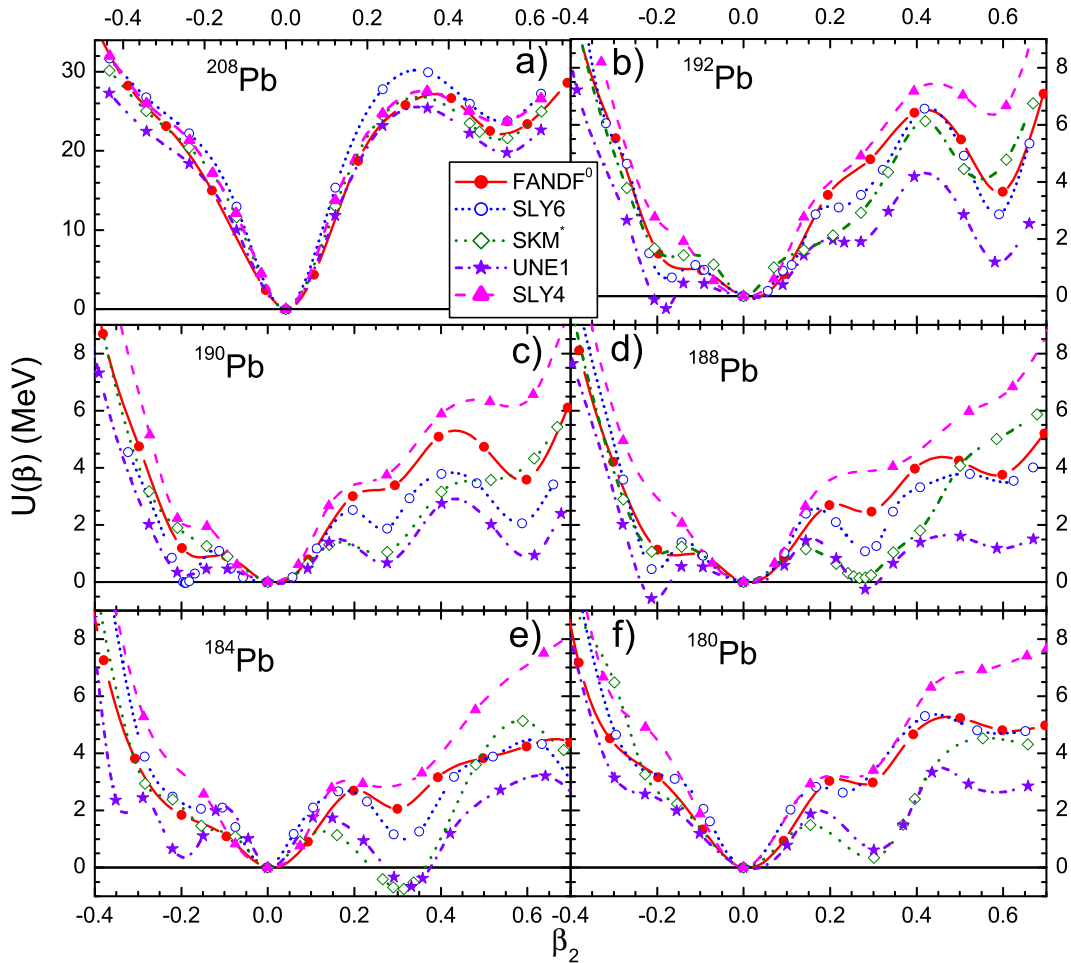


Figure 8. (Color online) Deformation energy curves $U(\beta)$ for Pb isotopes as a function of deformation β for FaNDF⁰ and various Skyrme EDFs. Shown are ^{208}Pb (a), ^{192}Pb (b), ^{190}Pb (c), ^{188}Pb (d), ^{184}Pb (e), and ^{180}Pb (f).

comparison with the doubly magic ^{208}Pb , shown in panel (a). All four curves behave in a similar way which corresponds to very rigid nature of this nucleus. Position of the first barrier and the second minimum are almost the same for all of the EDFs. For the small deformation region FaNDF⁰ and UNEDF1 curves show very similar behavior. The SkM* deformation energy curve seems to be the closest one to FaNDF⁰, and only SLY6 deformation energy is notably higher by $4 \div 5$ MeV at $\beta_2 = 0.3 \div 0.6$.

Next, we investigate the light isotopes which are of our main interest in the present work. For ^{192}Pb nucleus, shown in figure 8, panel (b), the FaNDF⁰ deformation energy follows rather closely to SLY6 and SkM* ones, being rather rigid at the minimum of $\beta = 0$. Only the UNEDF1 curve behaves softer predicting an oblate, $\beta_2 \simeq -0.2$, ground state. The SLY4 EDF is the most rigid. The latter is true also for the ^{190}Pb nucleus, shown in panel (c). The behavior of the FaNDF⁰ curve here is also rather rigid but softer compared to ^{190}Pb . It has a shallow minimum, roughly 1 MeV above the ground state energy, at $\beta_2 \simeq -(0.1 \div 0.2)$. According to the rest three Skyrme EDF predictions,

this nucleus is much softer. All of the corresponding Skyrme functions possess clearly distinguishable minima at the prolate deformation, $\beta_2 \simeq 0.3$. Corresponding excitation energies are about 2 MeV for SLy6, 1 MeV for SkM* and only 0.5 MeV for the UNEDF1 EDF. For oblate deformations, UNEDF1 and SLy6 EDFs lead to very low minima at $\beta_2 \simeq -0.2$, the latter being a little lower than the spherical one. As mentioned, these predictions are based on the single-reference mean-field level. Corrections to this scheme leads to a restoration of the spherical form for this nucleus [56].

In ^{188}Pb nucleus, shown in panel (d) of figure 8, the situation is similar, but now both of the deformed UNEDF1 minima are lower compared to the spherical one. The SkM* minimum is higher than the spherical one but only a bit. The FaNDF⁰ curve is qualitatively similar to the SLy6 one being a little more rigid. In the ^{184}Pb , shown in panel (e), SkM* and UNEDF1 EDFs predict a prolate ground state at $\beta_2 \simeq 0.3$. At last, the ^{180}Pb nucleus, shown in panel (f), becomes much more rigid than nuclei considered above.

To conclude this section, predictions of different Skyrme EDFs for light lead isotopes are found to be quite different. The SLy4 EDF is the most rigid of all functionals under consideration including FaNDF⁰. On the other hand, FaNDF⁰ predicts spherical form for all the lead isotopes. This could be explained with influence of the denominator of Eq. (24) which provides some feedback preventing the deformation of the light Pb isotopes. At the same time, FaNDF⁰ predictions are rather close to SLy6 ones, with exception of the ^{190}Pb nucleus.

5. Conclusion

This work presents the first application of the Fayans functional FaNDF⁰ [9] to deformed nuclei. Fayans functional makes an interesting alternative for Skyrme EDF with some promising properties, as shown in the current work. A systematic comparison for the mean-field deformations and deformation energies were made to two modern Skyrme EDFs: HFB-17 and HFB-27. Results were calculated for the uranium and lead isotopic chains. In the uranium case, our results are qualitatively close to both, the HFB-17 and HFB-27 functionals.

To check applicability of the Fayans functional for description of large deformation, we calculated the deformation energy curve for ^{238}U nucleus with FaNDF⁰, and four different Skyrme EDFs. Our result turned out to be rather close to SkM* and UNEDF1 ones. These two Skyrme parameterizations, in particularly UNEDF1, after inclusion of the octupole deformation and tri-axiality, reproduce values of the experimental first and second barriers in this nucleus sufficiently well [48]. Here, in the present work we limit ourselves with the quadrupole deformation only due to limitations of the used computer code. For the ^{238}U , the results obtained in axial framework for FaNDF⁰ are rather close to those of most successful Skyrme EDFs. Nevertheless, with the current calculation scheme, it is too early to draw any concrete conclusions about the fission properties of FaNDF⁰.

For the lead isotopes, however, there was some notable differences between FaNDF⁰ and Skyrme EDFs. Here, both of the HFB functionals predict strong deformation of the light isotopes: $A = 178 \div 196$ for the functional HFB-17 and $A = 178 \div 194$ for the HFB-27. This does not agree to experimental data on the charge radii [20] and magnetic moments [21, 22]. On the contrary, the Fayans functional predicts spherical mean-field solution for all Pb isotopes, in agreement with experimental trend. To examine these differences, we calculated deformation energy curves for several light lead isotopes. Again the FaNDF⁰ results are compared to those obtained with four Skyrme EDFs. Predictions of different Skyrme EDFs are quite different, the FaNDF⁰ ones being rather close to those of the SLy6 EDF.

Thus, the FaNDF⁰ functional, with the parameters adjusted to spherical nuclei, seems to describe rather well the ground state deformation properties of two isotopic chains studied in the present work. This feature may be linked to a peculiar density dependence of the Fayans functional, resulting from the energy dependence effects of the self-consistent TFSS [19] which are hidden in the formulation in terms of the EDF. A systematic analysis of deformed nuclei with the Fayans functional is necessary to estimate its possible benefits across larger portions of the nuclear chart. Also, to address the fission properties of the FaNDF⁰, fully tri-axial calculations are required.

6. Acknowledgments

We are grateful to Michael Bender for useful comments. The work was partly supported by the Grant NSh-932.2014.2 of the Russian Ministry for Science and Education, by the RFBR Grants 12-02-00955-a, 13-02-00085-a, 13-02-12106_ofi-m, 14-02-00107-a, 14-22-03040_ofi-m, the Grant by IN2P3-RFBR under Agreement No. 110291054, and Swiss National Scientific Foundation Grant No. IZ73Z0_152485 SCOPES. This work was also supported (M.K.) by Academy of Finland under the Centre of Excellence Programme 2012–2017 (Nuclear and Accelerator Based Physics Programme at JYFL) and FIDIPRO programme; and by the European Unions Seventh Framework Programme ENSAR (THEXO) under Grant No. 262010.

References

- [1] Vautherin D and Brink D M 1972 *Phys. Rev. C* **5** 626
- [2] Dechargé J and Gogny D 1980 *Phys. Rev. C* **21** 1568
- [3] Ring P 1996 *Prog. Part. Nucl. Phys.* **37** 193
- [4] Ring P and Schuck P 1980 *The Nuclear Many-Body Problem* (Springer-Verlag, New York).
- [5] M. Bender, Heenen P-H and Reinhard P-G 2003 *Rev. Mod. Phys.* **75** 121 .
- [6] Smirnov A V, Tolokonnikov S V and Fayans S A 1988 *Sov. J. Nucl. Phys.* **48** 995
- [7] Horen D J, Satchler G R, Fayans S A and Trykov E L 1996 *Nucl. Phys. A* **600** 193
- [8] Borzov I N, Fayans S A, Kromer E, Zawischa D 1996 *Z. Phys. A* **355** 117
- [9] Fayans S A 1998 *JETP Letters* **68** 169
- [10] Fayans S A, Tolokonnikov S V, Trykov E L and Zawischa D 2000 *Nucl. Phys. A* **676** 49
- [11] Dobaczewski J, Carlsson B G and Kortelainen M 2010 *J. Phys. G: Nucl. Part. Phys.* **37** 075106
- [12] Gebremariam B, Duguet T and Bogner S K 2010 *Phys. Rev. C* **82** 014305
- [13] Kaiser N, Weise W 2010 *Nucl. Phys. A* **836** 256
- [14] Carlsson B G and Dobaczewski J 2010 *Phys. Rev. Lett.* **105** 122501
- [15] Gebremariam B, Bogner S K and Duguet T 2011 *Nucl. Phys. A* **851** 17
- [16] Stoitsov M, Kortelainen M, Bogner S K, Duguet T, Furnstahl R J, Gebremariam B and Schunck N. 2010 *Phys. Rev. C* **82** 054307
- [17] Goriely S, Chamel N. and Pearson J M 2009 *Phys. Rev. Lett.* **102** 152503
- [18] Goriely S <http://www-astro.ulb.ac.be/bruslib>
- [19] Khodel V A and Saperstein E E 1982 *Phys. Rep.* **92** 183
- [20] Saperstein E E and Tolokonnikov S V 2011 *Phys. At. Nucl.* **74** 1277
- [21] Borzov I N, Saperstein E E and Tolokonnikov S V 2008 *Phys. At. Nucl.* **71**, 469
- [22] Borzov I N, Saperstein E E, Tolokonnikov S V, Neyens G and Severijns N 2010 *Eur. Phys. J. A* **45** 159
- [23] Tolokonnikov S V, Kamerdzhev S, Krewald S, Saperstein E E and Voitenkov D 2012 *Eur. Phys. J. A* **48** 70
- [24] Kamerdzhev S, Krewald S, Tolokonnikov S S. V. , Saperstein E E and Voitenkov D 2012 *Eur. Phys. J. Web of Conferences* **38** 10002
- [25] Tolokonnikov S V, Kamerdzhev S, Voitenkov D, Krewald S and Saperstein E E 2011 *Phys. Rev. C* **84** 064324
- [26] Tolokonnikov S V, Kamerdzhev S, Krewald S, Saperstein E E and Voitenkov D 2012 *Eur. Phys. J. Web of Conferences* **38** 04002
- [27] Borzov I N 2006 *Nucl. Phys. A* **777** 645
- [28] Gnezdilov N V, Borzov I N, Saperstein E E, and Tolokonnikov S V 2014 *Phys. Rev. C* **89** 034304
- [29] Migdal A B 1967 *Theory of finite Fermi systems and applications to atomic nuclei* (Nauka, Moscow, 1965; Wiley, New York).
- [30] Fayans S A and Khodel V A 1973 *JETP Lett.* **17** 444
- [31] Saperstein E E, Tolokonnikov S V 1998 *JETP Lett.* **68** 553
- [32] Kohn W and Sham L J 1965 *Phys. Rev.* **140** A1133
- [33] Oliveira L N, Gross E K U and Kohn W 1988 *Phys. Rev. Lett.* **60** 2430
- [34] Belyaev S T, Smirnov A V, Tolokonnikov S V, Fayans S A 1987 *Sov. J. Nucl. Phys.* **45** 783
- [35] Dobaczewski J, Flocard H and Treiner J 1984 *Nucl. Phys. A* 422 103
- [36] Hohenberg P and Kohn W 1964 *Phys. Rev.* **136** B864
- [37] Dobaczewski J, Stoitsov M V, Nazarewicz W and Reinhard P-G 2007 *Phys. Rev. C* **76** 054315
- [38] Lacroix D, Duguet T and Bender M 2009 *Phys. Rev. C* **79** 044318
- [39] Bender M, Duguet T and Lacroix D 2009 *Phys. Rev. C* **79** 044319
- [40] Satuła W, Dobaczewski J, Nazarewicz W and Rafalski M 2011 *Int. J. Mod. Phys.* **E20** 244
- [41] Tolokonnikov S V and Saperstein E E 2010 *Phys. At. Nucl.* **73** 1684
- [42] Stoitsov M V, Schunck N, Kortelainen M, Michel N, Nam H, Olsen E, Sarich J and Wild S 2013

Comp. Phys. Comm. **184** 1592

- [43] Friedman B and Pandharipande V R 1988 *Nucl. Phys.* **48** 995
- [44] Nolen J A, Schiffer J P 1969 *Annu. Rev. Nucl. Sci.* **19**
- [45] Brown B A 1998 *Phys. Rev. C* **58** 220
- [46] Goriely S, Hilaire S, Koning A, Sin M and Capote R 2009 *Phys. Rev. C* **79** 024612
- [47] Staszczak A, Baran A, Dobaczewski J, Nazarewicz W 2009 *Phys. Rev. C* **80** 014309
- [48] Kortelainen M, McDonnell J, Nazarewicz W, Reinhard P-G, Sarich J, Schunck N, Stoitsov M V and Wild S M 2012 *Phys. Rev. C* **85** 024304
- [49] McDonnell J D, Nazarewicz W and Sheikh J A 2013 *Phys. Rev. C* **87** 054327
- [50] Chabanat E, Bonche P, Haensel P, Meyer J and Schaeffer R 1998 *Nucl. Phys. A* **635** 231
- [51] Bartel J, Quentin P, Brack M, Guet C and Håkansson H B 1982 *Nucl. Phys. A* **386** 79
- [52] Bürvenich T, Bender M, Maruhn J and Reinhard P.-G 2004 *Phys. Rev. C* **69** 014307
- [53] Stoitsov M V, Dobaczewski J, Nazarewicz W, Pittel S and Dean D J 2003 *Phys. Rev. C* **68** 054312
- [54] Erler J, Birge N, Kortelainen M, Nazarewicz W, Olsen E, Perhac A M and Stoitsov M 2012 *Nature* **486** 509
- [55] Rodríguez-Guzmán R R, Egido J L and Robledo L M 2004 *Phys. Rev. C* **69** 054319
- [56] Bender M, Bonche P, Duguet T and Heenen P-H 2004 *Phys. Rev. C* **69** 064303
- [57] Audi G, Wapstra A H and Thibault C 2003 *Nucl. Phys. A* **729** 337